Thesis for the Degree of Master of Engineering

Nanoporous Membrane Composed of Block Copolymers and Au Nanoparticles for Catalytic Reaction

by
Limpat Nulandaya

Department of Polymer Engineering
The Graduate School
Pukyong National University

February 2019

Nanoporous Membrane Composed of Block Copolymers and Au Nanoparticles for Catalytic Reaction

Advisor: Prof. Yoo Seong Il

by

Limpat Nulandaya

A thesis submitted in partial fulfillment of the requirements for the degree of

Master Engineering

in Department of Polymer Engineering, The Graduate School,

Pukyong National University

Busan, South Korea

February 2019

Nanoporous Membrane Composed of Block Copolymers and Au Nanoparticles for Catalytic Reaction

A thesis

by

Limpat Nulandaya

Approved by:

Prof. Choi U Hyeok

Prof. Kim Joo Hyun

Prof. Yoo Seong Il

January 2019

CONTENTS

LIST OF FIGURES

Nanoporous Membrane Composed of Block Copolymers and Au Nanoparticles for Catalytic Reaction

Nulandaya Limpat

Department of Polymer Engineering

The Graduate School

Pukyong National University

Abstract

Non-solvent induced phase separation (NIPS) method has attracted many interests for fabrication of nanoporous block copolymer membranes with tunable pore size and cross-sectional morphologies. However, in most cases, asymmetric membranes are more dominated by irregular macropores in the bottom than nanopores in the top. Therefore this research is focus on symmetric membrane fabrication with fully nanoporous structure in the cross-section. Parameters such as doctor blade cast thickness, evaporation temperature and time were optimized. The obtained membranes have nanoporous structure where the main framework is built by PS block and coated by P2VP block on the surface. Since the P2VP block can be coordinated by $HAuCl_4$ as a precursor, further citrate reduction led to formation of Au nanoparticles inside the membrane. The catalytic reactivity was perform by reduction of 4-NP.

Keywords: PS-b-P2VP, NIPS method, AuNP composites

블록공중합체와 금 나노입자로 구성된 나노기공성 멤브레인의 촉매반응 연구

Nulandaya Limpat

고분자공학전공
대학원
부경대학교

요약

비·용매 유도 상분리(NIPS) 방법은 조정 가능한 모공 크기와 단면적 형태에 의한 나노기공성의 블록 복합체 멤브레인 제작에 많이 이용되고 있다. 그러나 NIPS 방법을 통해 멤브레인을 합성하게 되면, 하단으로 갈수록 기공의 크기가 나노스케일에서 매크로스케일로 커지는 비대칭 구조를 가지게 된다. 따라서 본 연구에서는 나노 기공성 구조로 이루어진 대칭 멤브레인 제작에 초점을 두었다. 대칭 구조를 가지는 멤브레인 제작을 위해 닥터블레이드의 캐스팅 두께, 증발 온도, 증발 시간을 최적화 하였다. 이렇게 합성된 대칭 구조의 멤브레인은 PS 블록이 주 뼈대를 이루고 표면을 P2VP 블록이 덮고 있는 구조를 가진다. 그리고 합성된 멤브레인 내부에 금 나노입자를 형성시키기 위하여, P2VP 블록 $HAuCl_4$ 와 배위공유결합 시킨 후, 시트레이트 환원반응을 통해 멤브레인 내부에 금 나노 입자를 합성하였다. 시료의 촉매효과는 4-nitrophenol 의 환원반응을 통하여 평가하였다.

키워드: PS-b-P2VP, NIPS 방법, AuNP 복합 재료

Chapter I. Introduction

Membrane plays important role in recent daily life. This term can be found in chemical or biological or even mechanical topics. An example in biological study is cell membrane and it is formed naturally. To make a simple discussion, in this research it is specify as a thin film for separation purpose. Membranes can be classified into symmetric and asymmetric based on the cross-section. Here we focus on symmetric membrane that means the identical structure from the top to bottom. The other challenging goals in membrane research are pore morphology, as well as its reproducibility.

I-1. Non-Solvent Induced Phase Separation

Non-solvent induced phase separation (NIPS) is one of the well-known method to obtain uniform porous membrane. This method mostly generates asymmetric cross section structure, but the symmetric [1] is also possible. Further research on cross section has also been reported [2]. In some conditions, self-assembly phenomena could be also involved in the process to form self-

assembly non-solvent induced phase separation (SNIPS). Membranes by SNIPS method are usually fabricated from diblock copolymer due to its two different block properties with strong connection.

First reported NIPS process was started from casting polymer solution 200 µm thickness on a glass plate, followed by partial solvent evaporation for 10 s, and then immersion in non-solvent (also known as precipitant) bath and finally dried in ambient conditions [3]. The SEM Image of this membrane is presented in Figure 1. Some explorations in polymer solution, casting condition and post-treatment have been done to produce porous membranes with various size and shape. For more various applications, the NIPS method is also reported to be formed in hollow fiber [4]–[8]. The doctor blade casting is also reported that it could be replaced with spray-coating and dip-coating [9].

Membrane formation by NIPS method has been explained by three phase diagram that is depicted in Figure 2 [10]. The key of formation is the transformation from liquid phase into a solid phase

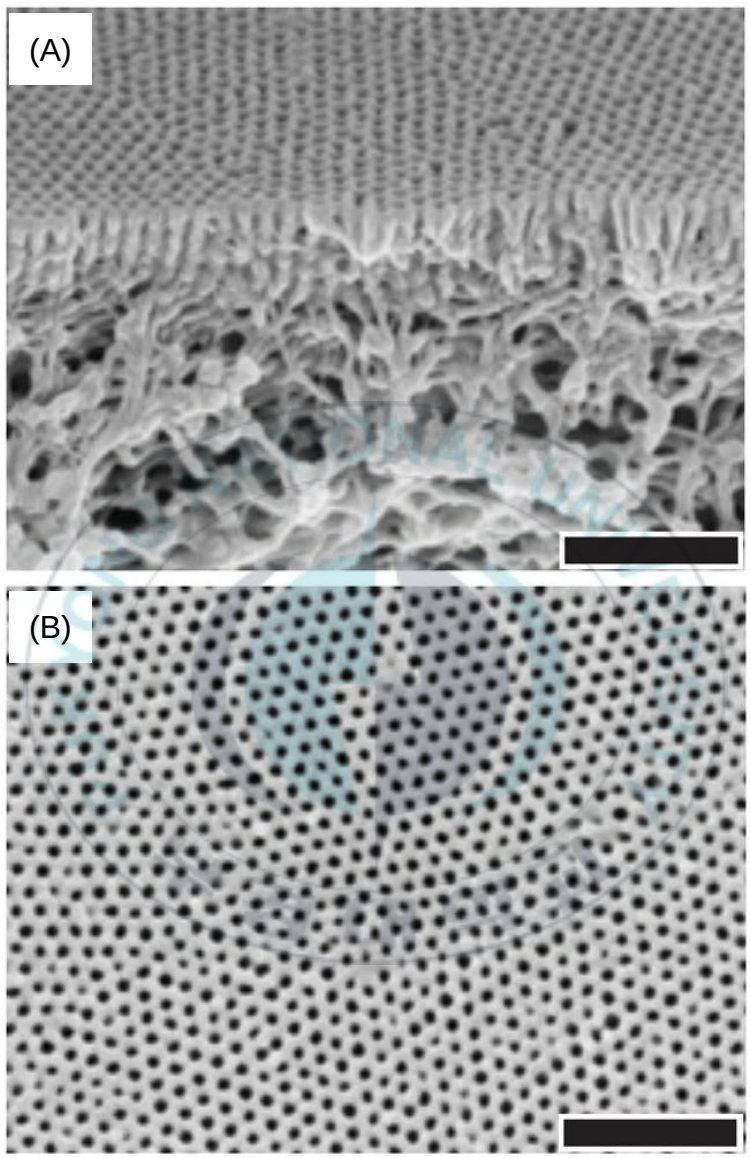

Figure 1 SEM images from asymmetric PS-b-P4VP diblock-copolymer film from: (A) edge view and (B) top view [3].

by the addition of precipitant in polymer and solvent mixture system. The correct composition will produce a well-arranged porous solid which is in the thin form called membrane. In more details, as shown in Figure 2A, initially casting solution has composition at t_0. During partial solvent evaporation, a concentration gradient can be built up perpendicular to the film surface. After the film is frozen by immersion in non-solvent, membrane has dense layer with x_1 composition on the top and coarsens structure to bottom, for example with x_2 and x_3, as shown in Figure 2B.

Some adjustments for solvent evaporation time plays important rule on the pore generation [11]–[15]. Kinetic studies of evaporation for the pore formation have been deeply examined using SAXS [15]–[17]. A lattice Monte Carlo simulations have also been conducted to study of fast and slow solvent evaporations [18]. Moreover, by controlling the solvent nature and evaporation time, a symmetric membrane could be produced [1] as presented in Figure 3. Not only symmetric structure, sponge-like and finger-like structures, as can be seen in Figure 4, could be also obtained by tuning evaporation time [19]. Another research has tried to use elevated temperature

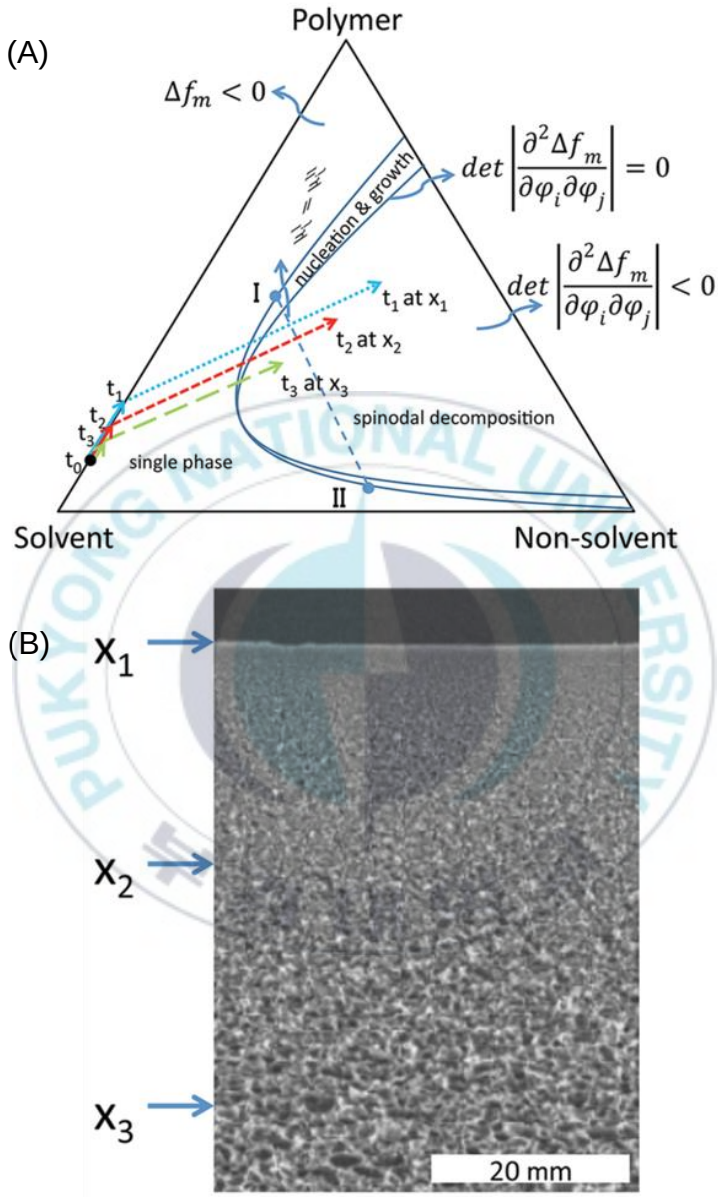

Figure 2 (A) Schematic of a ternary phase diagram of a polymer, solvent, and non-solvent and (B) a typical example of integral asymmetric membrane in cross sectional view [20].

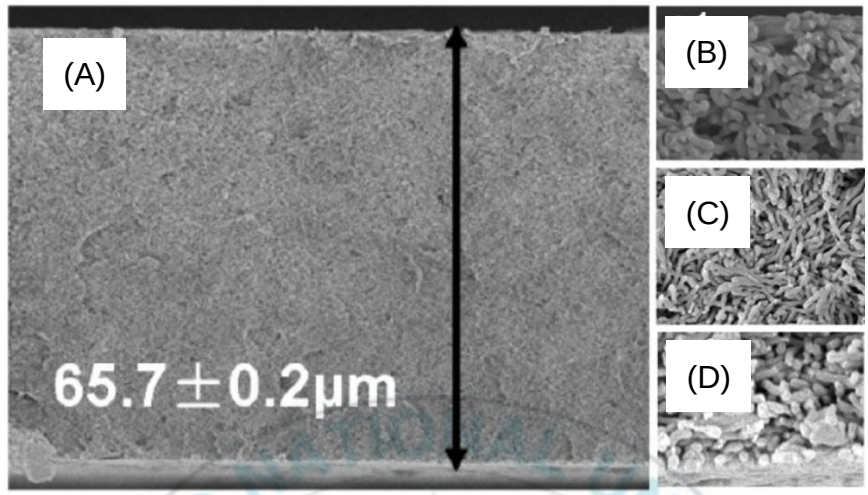

Figure 3 SEM images from symmetric PS-b-P4VP diblock-copolymer film from: (A) cross sectional view, (B) close to upper surface, (C) middle, and (D) close to bottom surface [1].

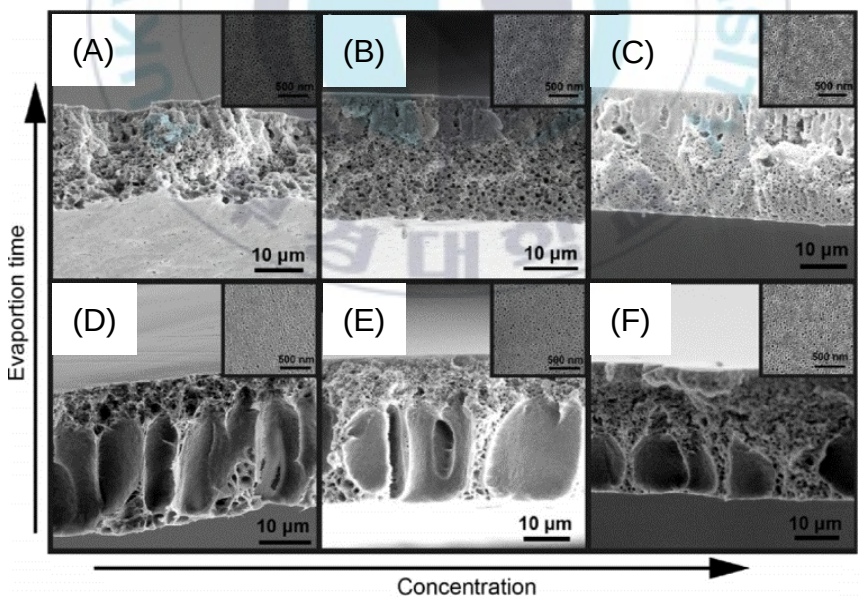

Figure 4 Cross sectional SEM images from (A,D) 9 wt%, (B,E) 10 wt%, and (C,F) 11 wt% with evaporation time (A-C) 60 s and (D-F) 45 s [19].

to boost solvent evaporation to get hierarchical multi-scale pores [21]. Moreover, the relative humidity is an empirical parameter for pore formation, for example polystyrene-block-poy(2-hydroxyethyl methacrylate) in below 20% [22] and poly(isoprene-b-styrene-b-4-vinylpyridine) in 40-45% [23]. An advantage of this condition is that the membrane has a great potential for humidity sensor [24].

Polymer solutions with various diblock copolymers, mixture of solvents, and addition of additives have been used to fabricate the membranes that have specific optimization casting condition. Polymer concentration also contributes to the pore formation [25], [26]. This concentration affected the micelles form in the solution [27].

Solvent from single or mixture types is another important part for pore formation [1]. The effect could also be seen from hydrodynamic radii of the dilute concentration polymer with various solvents [28]. Acetonitrile, Chloroform ($CHCl_3$), 1,4-dioxane (DOX), N,N-dimethylformamide (DMF), N,N-dimethylacetate (DMAc), and tetrahydrofuran (THF) are common

solvents for diblock copolymers. The mixture composition of DMF and THF also influences the pore dimension that was observed from the Debye-Scherrer ring [16] or cryo-SEM [12], [29].

Moreover, the using of polymer solution additives have also demonstrated by 3,5-Dihydroxybenzyl Alcohol (DHBA) [30], 9-Anthracenemethanol (AM) [30], Rutin (Ru) [30], Terephthalic acid (TPA) [30], Mellitic Acid (MA) [30], 1,3,5-tris(4'carboxy[1,1'-biphenyl]-4-yl)benzene (Tris) [30], α-cyclodextrine [31], α-(D)-glucose [31], saccharose [31], cobalt(II) acetate ($Co(Ac)_2$) [25], nickel(II) acetate ($Ni(Ac)_2$) [25], iron(II) acetate ($Cu(Ac)_2$) [25], copper(II) acetate ($Cu(Ac)_2$) [25], [32], copper(II) chloride ($CuCl_2$) [17], Magnesium Acetate ($Mg(Ac)_2$) [33], imidazole [34], and various type of ionic liquids [35]. Non-solvent pH [29], temperature [12], and type[21] are also contributing to the generated pores.

I-2. Block Copolymer

Block copolymer is a copolymer from two or more monomer cluster that form 'blocks' of repeating units. Each block in block copolymer has different property that is connected by strong covalent bond.

This incompatibility could lead self-assembly to form various crystal-like ordered microphase morphologies. The common membrane morphologies are spheres, cylinders, double gyroid and lamellae are shown in Figure 5 [20].

Besides widely used polystyrene-*block*-poly(4-vinylpyridine) (PS-*b*-P4VP) and polystyrene-*block*-poly(2-vinylpyridine) (PS-*b*-P2VP), many block copolymers such as polystyrene-*block*-poly(ethylene oxide) (PS-*b*-PEO) [36], poly(styrene-*block*-methyl methacrylate) (PS-*b*-PMMA) [14], poly(styrene)-*block*-poly(acrylic acid) (PS-*b*-PAA) [37], polystyrene-*block*-poly(2-hydroxyethyl methacrylate) (PS-*b*-PHEMA) [22], poly(tert-butylstyrene)-*block*-poly(4-vinylpyridine) (PtBS-*b*-P4VP) [38], poly(4-trimethylsilylstyrene)-*block*-poly(4-vinylpyridine) (PTMSS-*b*-P4VP) [38], polystyrene-*block*-poly(solketal methacrylate) (PS-*b*-PSMA) [39], polystyrene-*block*-poly(glyceryl methacrylate) (PS-*b*-PGMA) [39], poly(α-methylstyrene)-*block*-poly(4-vinylpyridine) (PαMS-*b*-P4VP) [40], and poly(4-methylstyrene)-*block*-poly(4-vinylpyridine) (P4MS-*b*-P4VP) [40]. Even, the triblock copolymers,

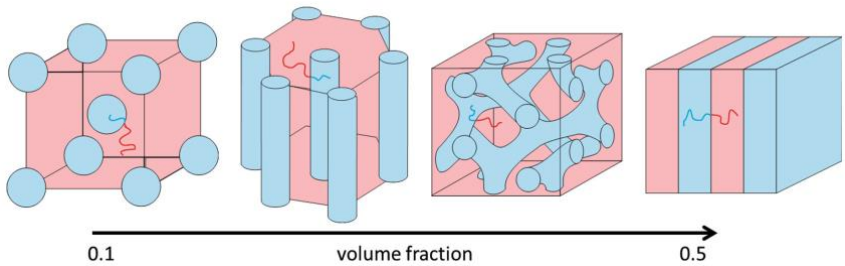

Figure 5 Various morphologies of diblock copolymer: spheres, cylinders, double gyroid, and lamellae [20].

polystyrene-*block*-poly(2-vinylpyridine)-*block*-poly(ethylene oxide) (PS-*b*-P2VP-*b*-PEO[13, 15, 41], poly(styrene-*block*-anthracene methyl methacrylate-*block*-methylmethacrylate) (PS-*b*-PAnMMA-*b*-PMMA) [42], poly(styrene-*block*-*tert*-butoxystyrene-*block*-styrene) (PS-*b*-PTBOS-*b*-PS) [34], poly(styrene-*block*-*tert*-hydroxystyrene-*block*-styrene) (PS-*b*-PHS-*b*-PS) [34], and poly(isoprene-*b*-styrene-*b*-(4-vinyl)-pyridine) [43] are also interesting for this membrane fabrication method. Mixture of two or more polymers including same diblock copolymer with different total molecular weights could also be used [37, 44, 45]. Further research also develops to use blend triblock copolymers [46]. The general trend is that using higher total molecular weight of diblock copolymer will generate bigger pore diameter in the membrane [47, 48]. Moreover, increased total molecular weight will decrease the polymer concentration and lead to thinner membrane [49].

I-3. Membrane Functionalization

A membrane could be further modified to get better adjust the pore. A post treatment method for adjusting the membrane pore was done

by electroless gold deposition [50]. Oxygen plasma treatment is also helpful to show hidden potential of the membrane pore [21]. Thermal annealing and urethane chemistry are also reported [22]. Alcohol swelling was potential to be used [51].

A membrane is usually used for separation by the pore size, but it could be modified to achieve more specific purposes [48]. A modification could also be performed to convert poly(4-vinyl pyridine) into poly(4-vinyl pyridine-N-oxide) that has better insolubility [52]. PS-b-P4VP with silver nanoparticle (AgNP) has good potential of anti-bacterial properties [53]. Incorporation with gold nano particles was also done for catalytic application [4]. A pH responsive membrane has been reported [52, 54]. A pH and thermo-double sensitivities membrane has modified by polydopamine coating and followed by the addition of pNIPAM-NH2 [55]. Further research has been conducted to prepare more hydrophilic membrane by ARGET ATRP [56]. Using specific block copolymer of anthracene methylmethacrylate, the obtained membrane could have photo-responsive behavior [42]. Carbon nanotubes is reported for enhancing humidity sensitivity [24]. Quaternization of the PS-b-

P4VP could be done for protein transport and separation [57].

In this regard, a preparation method for nanoporous membranes having isotropic structures by utilizing self-segregating properties of PS-b-P2VP copolymers was studied. The adjustment of evaporation conditions was carried out to control the nanoporous sizes and shapes. Furthermore, gold nanoparticles were synthesized inside nanoporous membrane to functionalize the surface. Then, the obtained composite catalytic activity was tested using a model of chemical reaction.

Chapter II. Experimental Section

II-1. Materials and Instruments

PS-b-P2VP diblock copolymer, that had average molecular weight of polystyrene and poly(2-vinylpyridine) were 440k and 353k kg/mol respectively with polydispersity index 1.05, was purchased from Polymer Source Inc., Canada. Ethanol, Tetrahydrofuran (THF) and N,N-Dimethylformaide (DMF) were purchased from Junsei. Diethyl malonate 99% was purchased from Alfa Aesar. All chemicals were used without further purification.

II-2. Membrane Fabrication via SNIPS

Typically, casting solution was prepared by dissolving PS-b-P2VP with mixed solvents of DMF and THF (1:1 wt.) until *c.a.* 10 wt.% of polymer concentration was reached. Diethyl Malonate 10 wt.% respect to the polymer was added to the polymer before adding the solvent to improve the mechanical strength of membrane. After the solution was completely dissolved, the cast was done on a glass (for doctor blade with a gap height of 200 μm) or a copper foil (for

doctor blade with a gap height more than 200 μm). The cast film were partially dried in room temperature followed by elevated temperature. Then, water was used as non-solvent to precipitate into a white membrane. Finally, the obtained white membranes were rinsed and dried between two sheets of tissues.

II-3. Composite Synthesis

A composite material was prepared from immersing nanoporous membrane in solution of gold chloride trihydrate 0.001 M. Subsequently, gold ions in nanoporous membrane was reduced into gold nanoparticles by sodium citrate 0.005 M at 60 ℃. Finally, the composite was obtained after washing with water to remove any non-reduced gold.

II-4. Characterization

The top, bottom and cross section morphologies were captured by a field emission scanning electron microscope (FESEM, TESCAN MIRA 3 LMH In-Beam Detector). The cross section of membrane were obtained from the cracked samples after dipping into liquid

nitrogen. The membranes were sputtered with thin Pt layer and observed under 3 kV of working voltage.

Composite and membrane were also characterized by Diffuse Reflectance Spectrophotometer (Diffuse Reflectance UV-Vis-NIR Spectrophotometer, SHIMADZU SolidSpec-3700). For this measurement, the samples were cut to a circle shape with diameter one inch. The reflectance wavelength was recorded from 240 to 1000 nm.

Chapter III. Results and Discussion

Composite of nanoporous membrane and gold nanoparticle is interesting for catalytic application[4] and nanoparticles filtration[50]. The presence of gold nanoparticles in membrane can decrease the pore size [50], thus utilizing large nanoporous membranes will address it. In this research, a high molecular weight polymer was chosen to synthesis nanoporous membranes.

III-1. Membrane Fabrication

Initially, a nanoporous membrane was fabricated following NIPS method where a concentrated dope of polymer solution is immersed into a non-solvent. Typical fabrication was done from high polymer concentration (c.a. 20 wt%) and initial thin cast condition (200 μm) [3]. However, in this research, challenges are found out from lower polymer concentration and thickness. Note, it was assumed that the concentration of dope solution is the most important in nanoporous formation. In this regard, elevated temperature evaporation (at 110 ℃) is proposed as booster to reach

the adequate concentration. Note, the evaporation temperature is higher than the boiling temperature of THF (66 ℃) but smaller than that of DMF (153 ℃). To confirm this idea, a membrane was fabricated with elevated temperature evaporation. At the same time, room temperature evaporation was used for another membrane fabrication.

SEM images of membrane from elevated temperature evaporation is demonstrated in Figure 6. This membrane has nanoporous structures only that is more clearly seen in higher magnification as shown in Figure 6A and open pore layer on the top membrane surface (Figure 6B). For comparison, membrane from room temperature evaporation was also characterized and the SEM images are arranged in Figure 7. As can be seen in Figure 7A, this membrane consists of nanoporous mainly in the top with mixture of microporous in the bottom. Moreover, dense skin layer on the top can also be observed on the top layer of cross sectional membrane morphology. This dense layer on the top cross section is related to the presence of close skin layer (Figure 7B). By comparing the results above, elevated temperature evaporation verified the

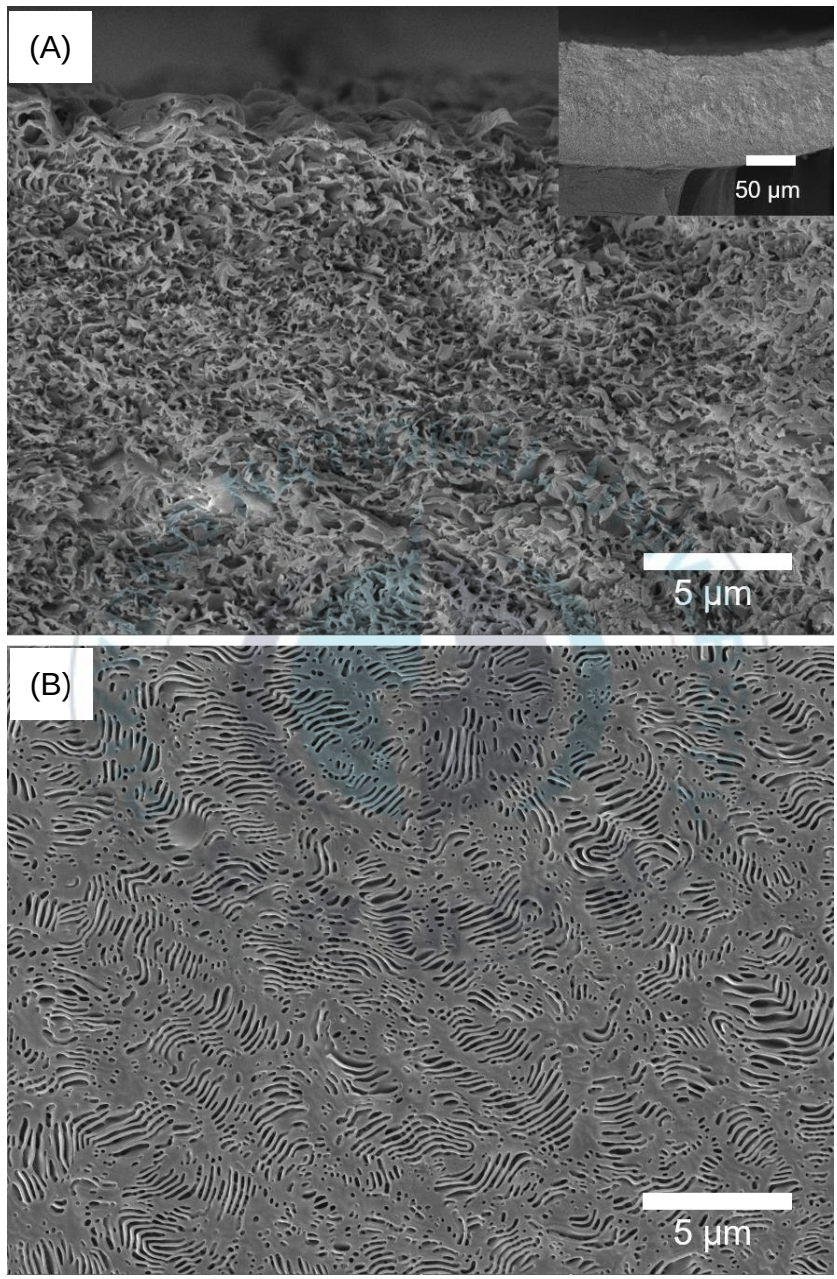

Figure 6 SEM images of membrane with elevated temperature evaporation in (A) cross section and (B) plane-view. (Insert image: full cross sectional view)

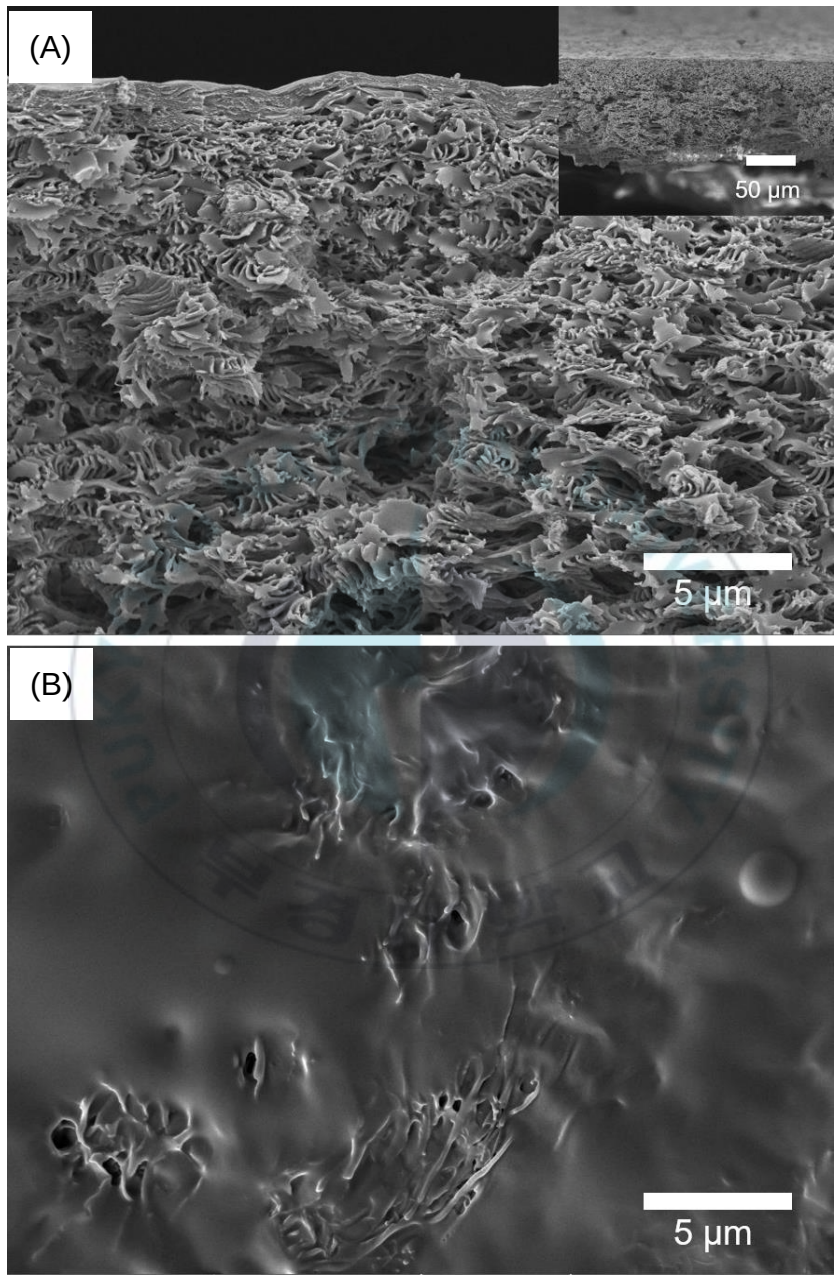

Figure 7 SEM images of membrane with room temperature evaporation in (A) cross section and (B) plane-view. (Insert image: full cross sectional view)

previous assumption as a good method for fabrication nanoporous membrane from high molecular weight of diblock copolymer.

Furthermore, plane view of nanoporous membrane in Figure 6A is used to calculate the pore size distribution. The black area in this image correspond to pore; therefore, measuring the black area by ImageJ sofware could generate the pore size distribution on the top membrane surface. The result is plotted in Figure 8A and the average pore diameter from this calculation is 122.90 ± 5.17 nm. Another measurement was performed by mercury porosimeter. The log differential intrusion against pore size is plotted in Figure 8B. The pores within this sample in range 1000 down to 100 nm was centered at about 202 nm. Membrane porosity could be also calculated and the result is approximately 59.32%. In addition, membrane bending in insert image shows that the nanoporous membrane is still flexible even the thickness is high.

To learn more about height control, the initial cast height and evaporation condition were adjusted. Firstly, the standard cast was chosen with initial height at 1000 μm and elevated room temperature

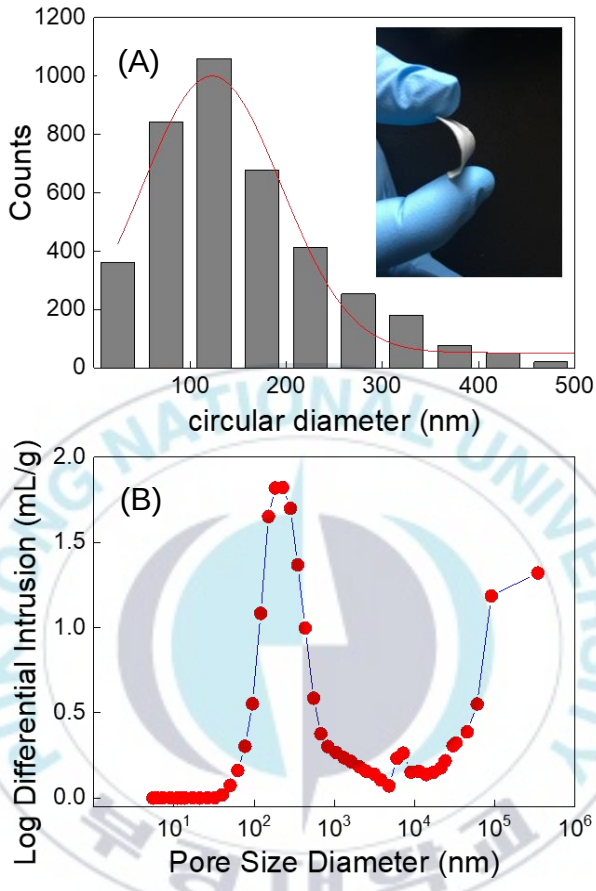

Figure 8 Pore size distribution of nanoporous membrane with elevated temperature evaporation from (A) plane-view SEM images and (B) mercury porosimetry (insert image: membrane flexibility test)

as explained previously. Then, higher initial cast condition at 1500 μm was applied. However, after drying, the final height was less than the standard membrane. From the SEM images in Figure 9A, it can be seen that the bottom part of membrane has macropores structure and the height is less than that of the standard cast. This is happened due to the non-homogenous evaporation rate especially in the middle cross section of this membranes. Physical observation showed that peeling of this membrane leaved white layer on substrate. Room temperature evaporation membrane was not fabricated from this initial height because of this failure.

Next, cast was done with lower initial height at 500 μm. Figure 9B and C shows the cross sectional view of membranes from elevated and room temperature evaporation, respectively. Membrane with elevated temperature evaporation has lower height than room temperature evaporation. The presence of microporous also can be seen clearly in the room temperature evaporation.

Lastly, the membrane was cast with initial height at 200 μm. In this condition, room temperature evaporation only could generate white

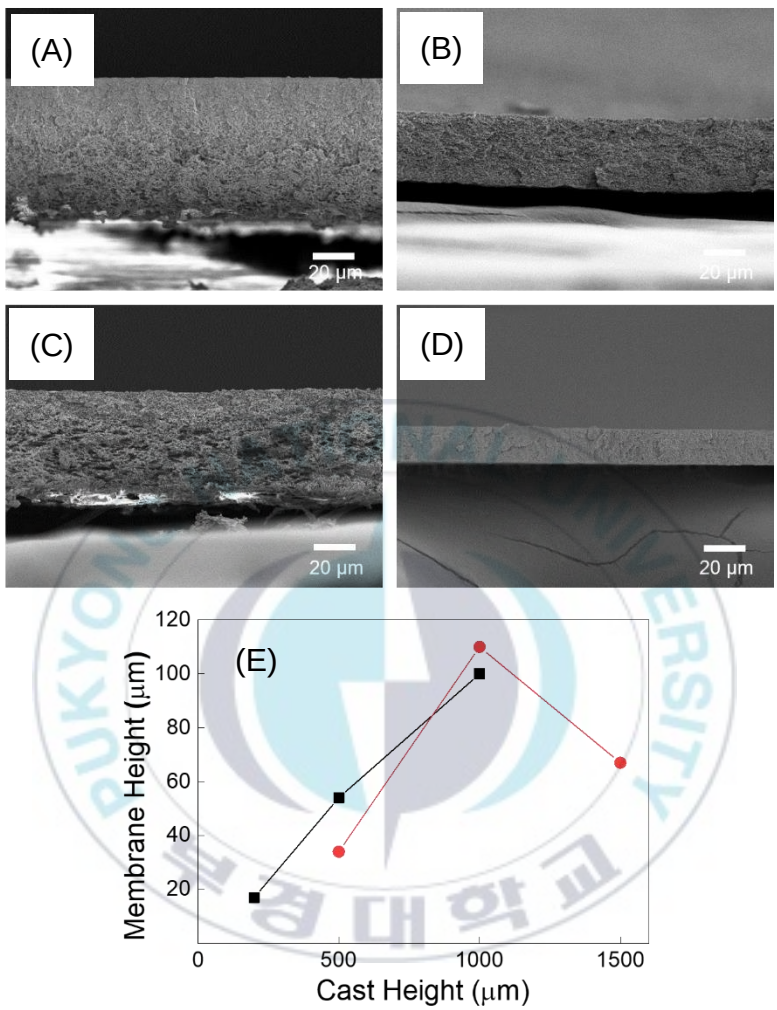

Figure 9 Cross sectional SEM image of membranes with evaporation at elevated temperature from initial cast height (A) 1500 and (B) 500 µm and at room temperature from initial cast height (C) 500 and (D) 200 µm. The membranes from 1000 µm is depicted in Figure III-1. (E) Summary of nanoporous membranes height from elevated temperature evaporation (red line with circle) and room temperature evaporation (black line with square).

membrane instead of transparent. Cross sectional images this membrane can be seen in Figure 9D. Summary of membranes height as a function of initial cast heights is plotted in the Figure 9E.

Figure 10 shows the plane view of this membranes. In the elevated temperature evaporation, open pore on top membranes surface can be formed (Figure 10A and B). On the other hand, close pore surface is found in membrane from initial cast height 500 μm with room temperature evaporation (Figure 10C). Moreover, less open pore can be obtained from initial cast height 200 μm with room temperature evaporation (Figure 10D). In this initial cast height, room temperature still has the appropriate solvent evaporation rate to open pore on the surface.

In NIPS membrane fabrication, evaporation time is an important empirical parameter. It is controlling the solvent composition in the mixture before immersion in water. Due to the presence of high solvent content and thin cast condition, various evaporation times (30, 40 and 70 s) were applied for membranes fabrication. From cross section image in Figure 11, it can be seen that the top to bottom

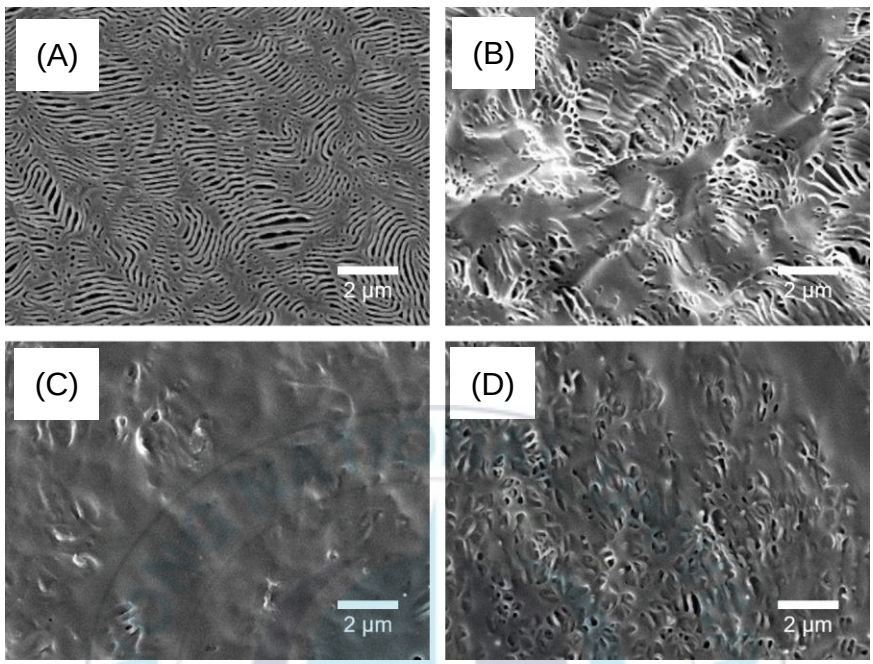

Figure 10 Plane view SEM images of membrane with evaporation at elevated temperature from initial cast height (A) 1500 and (B) 500 μm and at room temperature from initial cast height (C) 500 and (D) 200 μm. The membranes from 1000 μm is depicted in Figure III-1.

of membranes did not depend on evaporation time. However, the number of open pores on the top membrane surface is affected by this evaporation time variation. As it can be seen in Figure 11, increasing evaporation time will decrease the number of open pore on membrane surface. Again, the optimum open pore on top membrane surface was formed with elevated temperature evaporation for 30 s.

Open pore on top membranes surface via NIPS process are also influenced by humidity as an empirical parameter.[22], [23] In PS-b-P2VP membranes, P2VP block will interact with water molecule in the air and can inhibit a pore formation. In this regard, membranes were cast under relative humidity 40% and 85%. Plane view SEM image of these membranes can be seen in Figure 12. The optimum evaporation times were 20 and 10 s in relative humidity 40% and 85%, respectively.

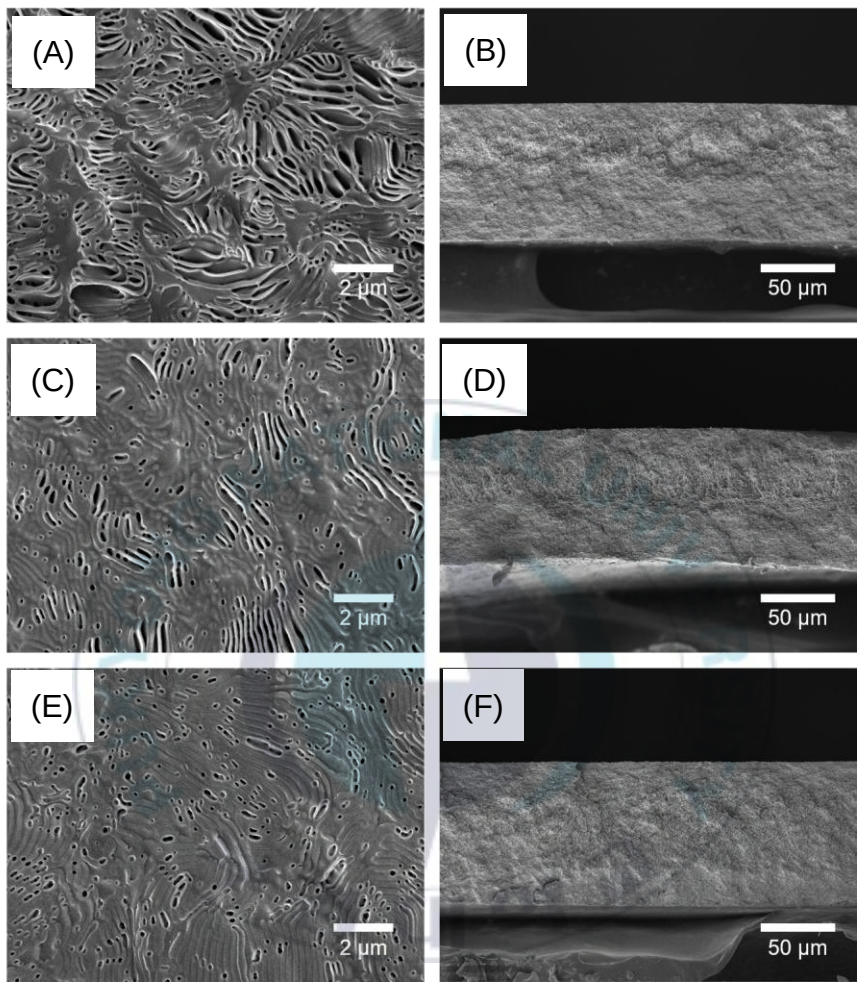

Figure 11 Plane view and cross sectional SEM images of membrane from elevated temperature evaporation for (A,B) 30 s, (C,D) 40 s, and (E,F) 70 s

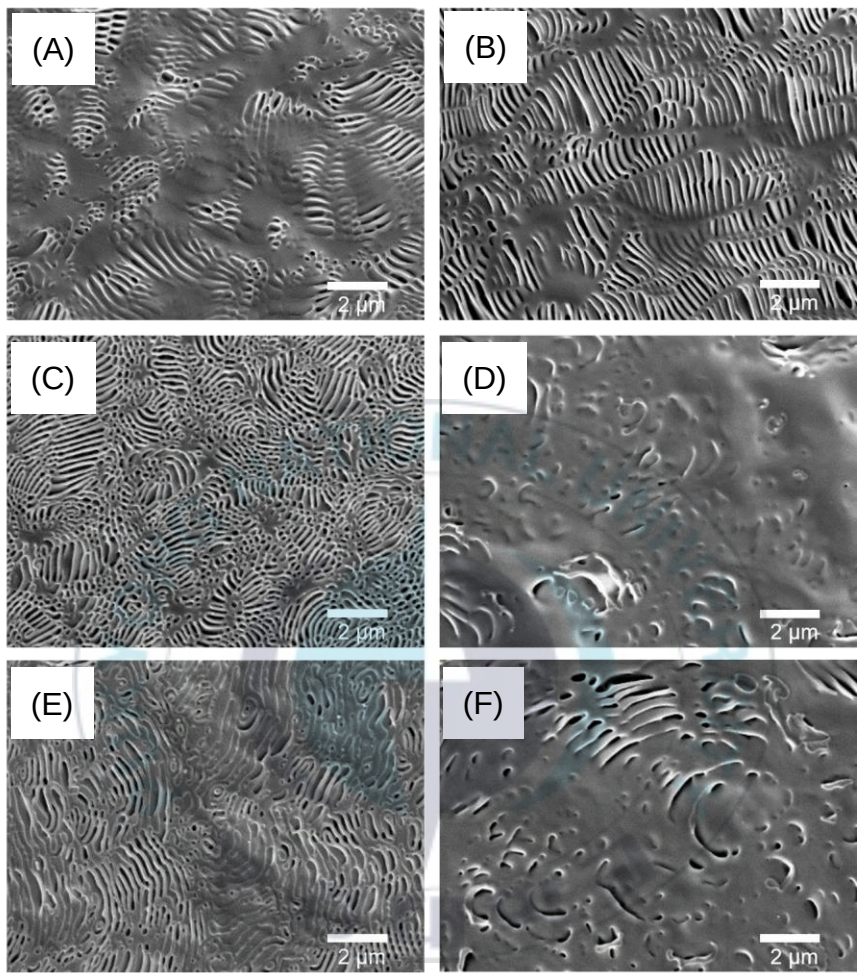

Figure 12 Plane view SEM images of membrane in relative humidity 40% and 85% with elevated temperature evaporation for (A,B) 10 s, (C,D) 20 s, and (E,F) 30 s.

III-2. Composite Fabrication

To fabricate a composite, gold nanoparticles were synthesized inside of the nanoporous membranes. The scheme in Figure 13A shows the formation of gold nanoparticles. Nanoporous membrane was immersed in $HAuCl_4$, as a gold nanoparticles precursor, for coordination with Nitrogen atom from P2VP blocks on the pore surface. Next, a sodium borohydride solution was used to reduce $HAuCl_4$ into gold nanoparticles; therefore, the gold nanoparticles were synthesized on the nanoporous membrane surface. This gold nanoparticles formation was further confirmed by SEM analysis. The nanoparticles on composite surface is identified as gold nanoparticles (as shown in Figure 13B), which is absence in the membrane surface. Gold nanoparticle was also found throughout membrane pore surface, even in the middle of membrane cross section as shown in Figure 13C.

In addition, composite and membranes were characterized using DRUV-Vis spectrophotometer to confirm the presence of gold nanoparticles. Membrane, which is white (Figure 14B), is reflecting

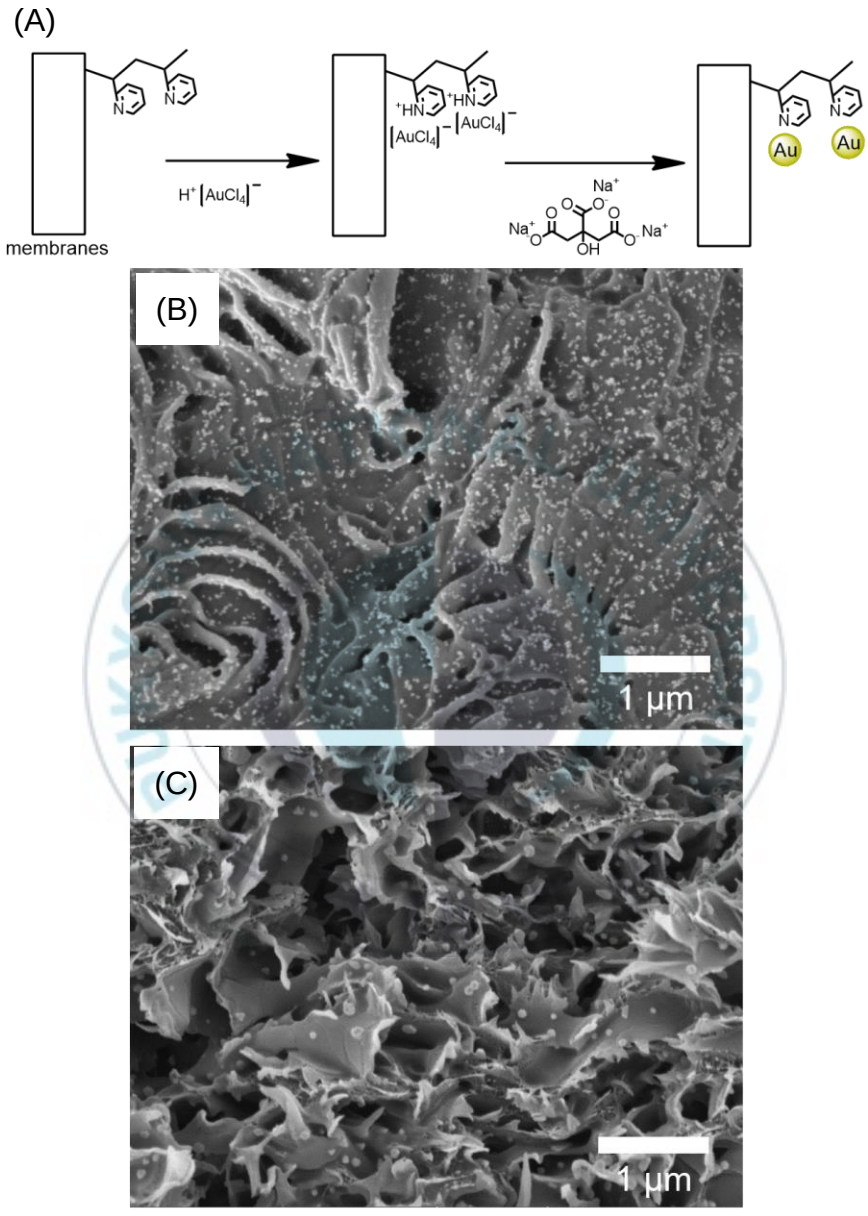

Figure 13 (A) Schematic of AuNP synthesis in membranes. Composite SEM images of (B) plane view and (C) cross section.

over 90% of photons in the visible wavelengths as shown with black line in Figure 14A. On the other hand, composite, with its dark color (Figure 14C), has reflectance below 10% as can be seen in red line in Figure 14A. This low reflectance in composite is confirmed that the gold nanoparticles is responsible for the photon absorption.

Initially, flux test of various solutions was performed on membrane and composite. Water filtration on membrane, as can be seen with square and black line in Figure 15A, shows that the flux is stable during 10 minutes filtration. Then, sodium borohydride solution was used for feed of filtration and the result was plotted in circle and red line. Even through there is a sudden increasing, the flux is decreasing close to water in the end. The final feed was mixture 4-nitrophenol, sodium borohydride and PS beads that has triangle and blue line in the Figure 15A. It can be seen that there is a small flux decreasing due to the pore blocking with PS beads.

On the other hand, flux test on composite has different profile than membrane as seen in Figure 15B. Flux for water filtration is same with membrane at around 90 L m^{-2} h^{-1}. However, in sodium

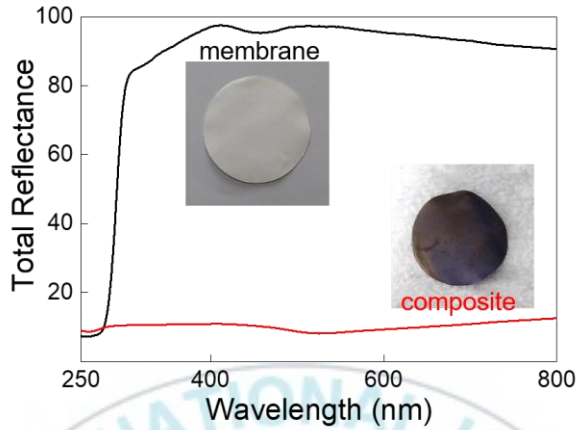

Figure 14 Diffuse reflectance UV-Vis spectroscopy of membrane (black line) and composite (red line). Insert images: photos of membrane and composite.

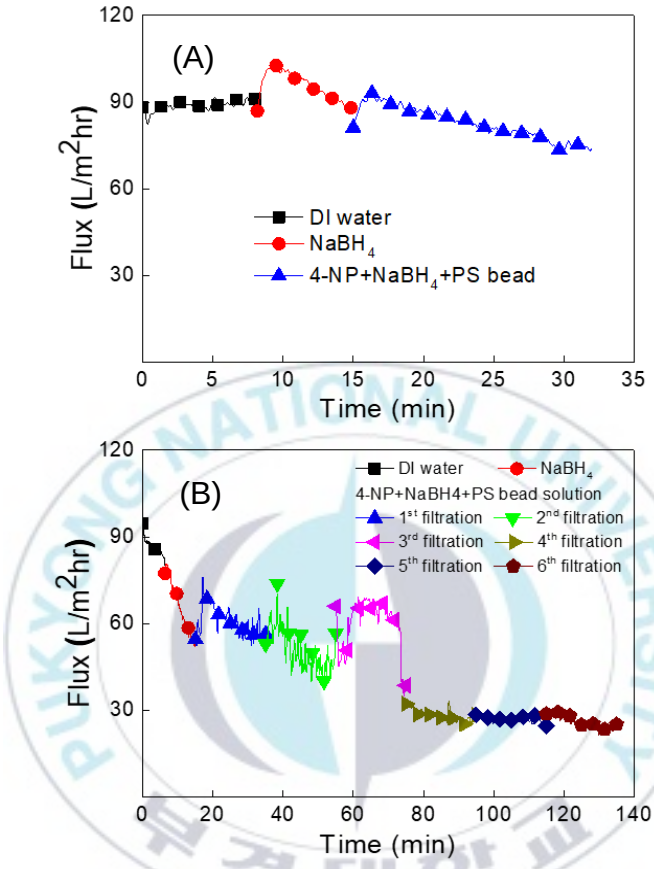

Figure 15 Flux measurement of DI water, sodium borohydride solution and pollutant model with (A) membrane and (B) composite.

borohydride feed, there is a significant drop of flux up to 60 L m^{-2} h^{-1}. It indicated that there is a pore size decreasing in composite. Further, mixture of 4-nitrophenol, sodium borohydride and PS beads is also decreasing in flux after some re-filtration. Started from the fourth filtration, the flux is stable at about 90 L m^{-2} h^{-1} that indicating there is no pore size decreasing from this filtration. Note, composite has gold nanoparticles that cannot be analyzed by mercury porosimetry due to amalgamation; therefore the decreasing pore size of composite just rely on the decreasing flux test. The re-filtration of this mixture will be discussed later.

For the catalytic activity test, the gold nanoparticles in composite are used to reduce 4-nitrophenol into 4-aminophenol as shown in Figure 16A. Due to the excess of sodium borohydride, 4-nitrophenol converts into 4-nitrophenolate ion that has strong peak at 400 nm. The feed and permeate are analyzed using UV-Vis spectrophotometer and the spectra are presented in Figure 16B. The absorbance at 400 nm is decreasing with repeated reaction filtration. The 4-nitrophenol degradation as function of filtration cycle number is depicted in Figure 16C. It can be seen that first filtration just

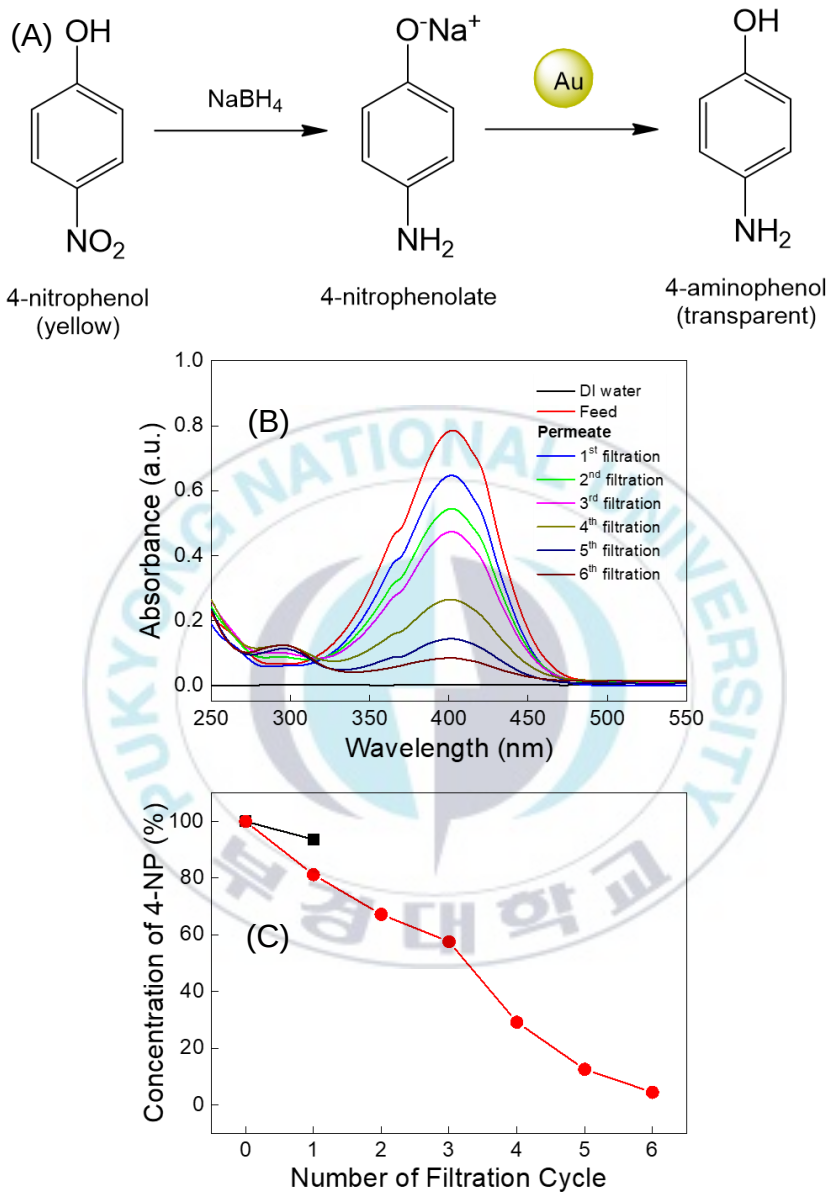

Figure 16 (A) Schematic reduction reaction of 4-nitrophenol inside membrane. UV Vis spectra of filtration solutions using (B) composite and (C) comparison of 4-nitrophenol removal by membrane (black) and composite (red).

reduces 4-nitrophenol up to 81.2% from the feed. Then, after six filtration cycle,the concentration of 4-nitrophenol can be reduced up to 4.4%.

To test the size dependent filtration, the 1 μm PS beads pollutant was added to feed for demonstration. Note, this size of PS beads is chosen based on the significant different size with the pore size of composite. Feed and permeate from composite filtration were qualitatively measured using fluorescence microscopy. The results bright field and fluorescence images are arranged in Figure 17. Based on the absence of dark and yellow green particles in the bright field and fluorescence images, respectively, it can be seen that the permeate (Figure 17C and D) doesn't contain PS beads. Compared to the feed (Figure 17A and B), it can be verified that the composite size filtration is successfully performed.

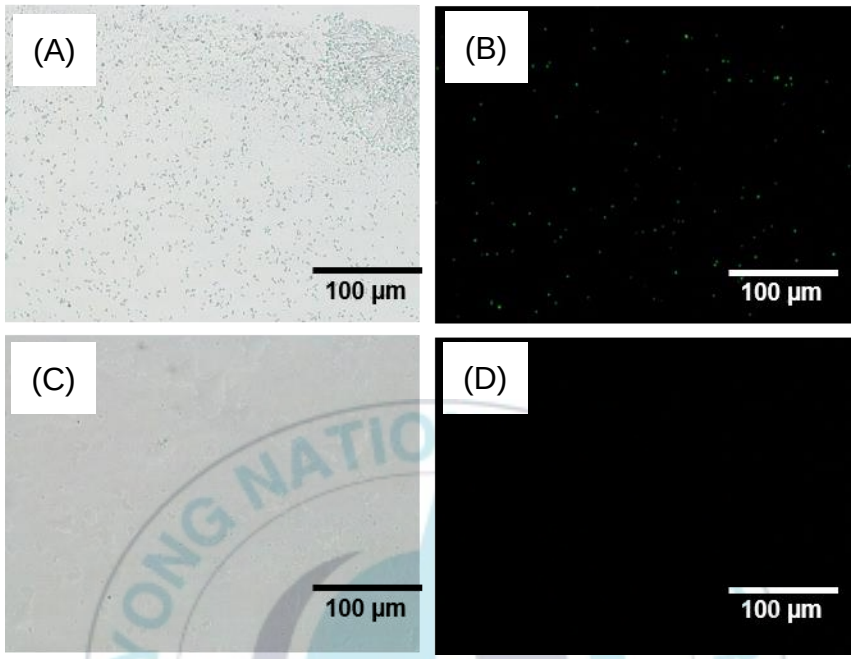

Figure 17 Bright field and fluorescence optical images of (A,B) feed and (C,D) permeate of composite.

Chapter IV. Conclusion

A nanoporous membrane from symmetrical diblock copolymer was successfully fabricated via NIPS process. The effect of evaporation temperatures and times played important role on the membranes formation. Additionally, composite of AuNPs inside membrane could be prepared and the chemical activity was presented by catalysing a model chemical reaction.

References

[1] Z. Yi, P.B. Zhang, C.J. Liu, and L.P. Zhu (2016), *Macromolecules*, **49**, 3343.

[2] L.P. Zhang, Y. M. Li, Y. Gu, R. M. Dorin, and U. Wiesner (2016), *Polymer*, **107**, 398.

[3] K.V. Peinemann, V. Abetz, and P. F. W. Simon (2007), *Nat. Mater.* **6**, 992.

[4] R. Hilke, N. Pradeep, P. Madhavan, U. Vainio, A. R. Behzad, R. Sougrat, S. P. Nunes, and K.V. Peinemann (2013), *ACS Appl. Mater. Interfaces*, **5**, 7001.

[5] S. P. Nunes, A. R. Behzad, and K. V. Peinemann (2013), *J. Mater. Res.*, **28**, 2661.

[6] M. Radjabian, J. Koll, K. Buhr, U. Vainio, C. Abetz, U. A. Handge, and V. Abetz (2014), *Polymer*, **55**, 2986.

[7] K. Sankhala, J. Koll, M. Radjabian, U. A. Handge, and V. Abetz (2017), *Adv. Mater. Interfaces*, **4**, 1600991.

[8] K. Sankhala, J. Koll, and V. Abetz (2018), *ACS Macro Lett.*, **7**, 840.

[9] J. Hahn, J. I. Clodt, C. Abetz, V. Filiz, and V. Abetz (2015), *ACS Appl. Mater. Interfaces*, **7**, 21130.

[10] H. Strathmann and K. Kock (1997), *Desalination*, **21**, 241.

[11] W. A. Phillip, R. M. Dorin, J. Werner, E. M. V. Hoek, U. Wiesner, and M. Elimelech (2011), *Nano Lett.*, **11**, 2892.

[12] A. Jung, S. Rangou, C. Abetz, V. Filiz, and V. Abetz (2012), *Macromol. Mater. Eng.*, **297**, 790.

[13] A. Jung, V. Filiz, S. Rangou, K. Buhr, P. Merten, J. Hahn, J. Clodt, C. Abetz, and V. Abetz (2013), *Macromol. Rapid Commun.*, **34**, 610.

[14] M. Karunakaran, R. Shevate, and K. V. Peinemann (2016), *RSC Adv.*, **6**, 29064.

[15] B. Sutisna, G. Polymeropoulos, V. Musteata, K. V. Peinemann, A. Avgeropoulos, D. M. Smilgies, N. Hadjichristidis, and S. P. Nunes (2016), *Mol. Syst. Des. Eng.*, **1**, 278.

[16] C. Stegelmeier, V. Filiz, V. Abetz, J. Perlich, A. Fery, P. Ruckdeschel, S. Rosenfeldt, and S. Forster (2014), *Macromolecules*, **47**, 5566.

[17] C. Stegelmeier, A. Exner, S. Hauschild, V. Filiz, J. Perlich, S. V. Roth, V. Abetz, and S. Förster (2015), *Macromolecules*, **48**, 1524.

[18] J. Hao, Z. Wang, Z. Wang, Y. Yin, R. Jiang, B. Li, and Q. Wang (2017), *Macromolecules*, **50**, 4384.

[19] Q. Zhang, Y. M. Li, Y. Gu, R. M. Dorin, and U. Wiesner (2016), *Polymer*, **107**, 398.

[20] V. Abetz (2015), *Macromol. Rapid Commun.*, **36**, 10.

[21] S. Yoo, J. H. Kim, M. Shin, H. Park, J. H. Kim, S. Y. Lee, and S. Park (2015), *Sci. Adv.*, **1**, e1500101.

[22] J. Wang, M. M. Rahman, C. Abetz, S. Rangou, Z. Zhang, and V. Abetz (2018), *Macromol. Rapid Commun.*, **39**, e1800435.

[23] Y. M. Li, Q. Zhang, J. R. Á lvarez-Palacio, I. F. Hakem, Y. Gu, M. R. Bockstaller, and U. Wiesner (2017), *Polymer*, **126**, 368.

[24] R. Shevate, M. A. Haque, F. H. Akhtar, L. F. Villalobos, T. Wu, and K. V. Peinemann (2018), *Angew. Chemie Int. Ed.*, **57**, 1.

[25] D. S. Marques, U. Vainio, N. M. Chaparro, V. M. Calo, A. R. Bezahd, J. W. Pitera, K. V. Peinemann, S. P. Nunes, U. Vainio, and K. V. Peinemann (2013), *Soft Matter*, **9**, 5557.

[26] S. Dami, C. Abetz, B. Fischer, M. Radjabian, P. Georgopanos,

and V. Abetz (2017), *Polymer*, **126**, 376.

[27] L. Oss-Ronen, J. Schmidt, V. Abetz, A. Radulescu, Y. Cohen, and Y. Talmon (2012), *Macromolecules*, **45**, 9631.

[28] M. Radjabian, C. Abetz, B. Fischer, A. Meyer, and V. Abetz (2017), *ACS Appl. Mater. Interfaces*, **9**, 31224.

[29] S. P. Nunes, M. Karunakaran, N. Pradeep, A. R. Behzad, B. Hooghan, R. Sougrat, H. He, and K. V. Peinemann (2011), *Langmuir*, **27**, 10184.

[30] P. Madhavan, K. V. Peinemann, and S. P. Nunes (2013), *ACS Appl. Mater. Interfaces*, **5**, 7152.

[31] J. I. Clodt, S. Rangou, A. Schröder, K. Buhr, J. Hahn, A. Jung, V. Filiz, and V. Abetz (2013), *Macromol. Rapid Commun.*, **34**, 190.

[32] S. P. Nunes, R. Sougrat, B. Hooghan, D. H. Anjum, A. R. Behzad, L. Zhao, N. Pradeep, I. Pinnau, U. Vainio, and K. V. Peinemann (2010), *Macromolecules*, **43**, 8079.

[33] M. Gallei, S. Rangou, V. Filiz, K. Buhr, S. Bolmer, C. Abetz, and V. Abetz (2013), *Macromol. Chem. Phys.*, **214**, 1037.

[34] B. Sutisna, G. Polymeropoulos, E. Mygiakis, V. Musteata, K. V. Peinemann, D. M. Smilgies, N. Hadjichristidis, and S. P. Nunes (2016), *Polym. Chem.*, **7**, 6189.

[35 P. Madhavan, R. Sougrat, A. R. Behzad, K. V. Peinemann, and S. P. Nunes (2015), *J. Memb. Sci.*, **492**, 568.

[36] J. Hahn, V. Filiz, S. Rangou, J. Clodt, A. Jung, K. Buhr, C. Abetz, and V. Abetz (2013), *J. Polym. Sci. Part B Polym. Phys.*, **51**, 281.

[37] H. Yu, X. Qiu, A. R. Behzad, V. Musteata, D. M. Smilgies, S. P. Nunes, and K. V. Peinemann (2016), *Chem. Commun.*, **52**, 12064.

[38] J. Hahn, V. Filiz, S. Rangou, B. Lademann, K. Buhr, J. I. Clodt, A. Jung, C. Abetz, and V. Abetz (2013), *Macromol.*

Mater. Eng., **298**, 1315.

[39] S. Saleem, S. Rangou, C. Abetz, B. Lademann, V. Filiz, and V. Abetz (2017), *Polymers*, **9**, 216.

[40 C. Höhme, J. Hahn, B. Lademann, A. Meyer, B. Bajer, C. Abetz, V. Filiz, and V. Abetz (2016), *Eur. Polym. J.*, **85**, 72.

[41] V. Musteata, B. Sutisna, G. Polymeropoulos, A. Avgeropoulos, F. Meneau, K. V. Peinemann, N. Hadjichristidis, and S. P. Nunes (2018), *Eur. Polym. J.*, **100**, 121.

[42 P. Madhavan, B. Sutisna, R. Sougrat, and S. P. Nunes (2016), *RSC Adv.*, **6**, 75594.

[43] R. M. Dorin, D. S. Marques, H. Sai, U. Vainio, W. A. Phillip, K. V. Peinemann, S. P. Nunes, and U. Wiesner (2012), *ACS Macro Lett.*, **1**, 614.

[44] M. Radjabian, and V. Abetz (2015), *Adv. Mater.*, **27**, 352.

[45] H. Yu, X. Qiu, N. Moreno, Z. Ma, V. M. Calo, S. P. Nunes, and K. V. Peinemann (2015), *Angew. Chemie Int. Ed.*, **54**, 13937.

[46] T. G. Haenelt, C. Abetz, and V. Abetz (2018), *Macromol. Chem. Phys.*, **219**, 1700241.

[47] S. Rangou, K. Buhr, V. Filiz, J. I. Clodt, B. Lademann, J. Hahn, A. Jung, and V. Abetz (2014), *J. Memb. Sci.*, **451**, 266.

[48] J. Hahn, J. I. Clodt, V. Filiz, and V. Abetz (2014), *RSC Adv.*, **4**, 10252.

[49] J. I. Clodt, B. Bajer, K. Buhr, J. Hahn, V. Filiz, and V. Abetz (2015), *J. Memb. Sci.*, **495**, 334.

[50] H. Yu, X. Qiu, S. P. Nunes, and K. V. Peinemann (2014), *Angew. Chemie Int. Ed.*, **53**, 10072.

[51] J. Yin, X. Yao, J. Y. Liou, W. Sun, Y. S. Sun, and Y. Wang (2013), *ACS Nano*, **7**, 9961.

[52] R. Shevate, M. Karunakaran, M. Kumar, and K. V. Peinemann (2016), *J. Memb. Sci.*, **501**, 161.

[53] P. Madhavan, P. Y. Hong, R. Sougrat, and S. P. Nunes (2014), *ACS Appl. Mater. Interfaces*, **6**, 18497.

[54] S. P. Nunes, A. R. Behzad, B. Hooghan, R. Sougrat, M. Karunakaran, N. Pradeep, U. Vainio, and K. V. Peinemann (2011), *ACS Nano*, **5**, 3516.

[55] J. I. Clodt, V. Filiz, S. Rangou, K. Buhr, C. Abetz, D. Höche, J. Hahn, A. Jung, and V. Abetz (2013), *Adv. Funct. Mater.*, **23**, 731.

[56] D. Keskin, J. I. Clodt, J. Hahn, V. Abetz, and V. Filiz (2014), *Langmuir*, **30**), 8907.

[57] X. Qiu, H. Yu, M. Karunakaran, N. Pradeep, S. P. Nunes, and K. V. Peinemann (2013), *ACS Nano*, **7**, 768.

Acknowledgements

First, I would like to thank to God due to His grace, this thesis could be done. In this work, one of the reminder is coming from Galatians 5:25 that “Since we live by the Spirit, let us keep in step with the Spirit.”.

Then, my best gratitude is presented for my advisor, Prof Seong Il Yoo, due to his never ending helps and supports. Also, especially for the members of the soft and nano group, both past and present: Je Nam Jin, Song Chang Hyeon, Maulida Zakia, Merreta Noorenza Biutty, Lee Geon Seok, and Gu Ja Min, I would like to give my appreciation for the daily discussions and times.

Moreover, many thanks are also presented for my family in Indonesia. Although they are far away from Busan, their supports in permission, praying, and hope fill my whole days during this research. Finally, I am so grateful for my friends in South Korea, especially Busan who can not be mentioned one by one. Due to your present, I could enjoy my every single minutes.

Pukyong National University
Busan, South Korea

January 2019

Nulandaya Limpat